Faraday Discuss., 1996, **104**, 93–110

Simulation of homogeneous crystal nucleation close to coexistence

Pieter-Rein ten Wolde,*[,a] Maria J. Ruiz-Montero[b] and Daan Frenkel[a]

[a] *FOM Institute for Atomic and Molecular Physics, Kruislaan 407, 1089 SJ Amsterdam, The Netherlands*

[b] *Física Teórica, Facultad de Física, Apdo. de Correos 1065, 41080 Sevilla, Spain*

We discuss a numerical scheme to study homogeneous crystal nucleation. Using this approach, it is possible to compute the height of the free energy barrier that separates the solid from the liquid phase and the rate at which this barrier is crossed. We point out that there is a fundamental difference between the use of a global- and a local-order parameter to measure the degree of crystallinity. Using a global-order parameter, precritical nuclei may break up spontaneously for entropic reasons. Near the top of the barrier the nuclei combine to form a relatively large cluster. The transition from many small clusters to one large cluster is discussed in some detail. Finally we present a new method that allows us to avoid this entropic cluster break up.

1 Introduction

Homogeneous crystallization is an activated process. Small crystallites in the melt have to reach a critical size in order to grow into a crystal. The probability of forming a critical nucleus due to spontaneous fluctuations is determined by the excess energy of this nucleus.[1,2] In experiments, the height of this barrier is typically of the order of 75 k_BT.[1] This implies that, at any given instant, the density of critical nuclei is of the order of 1 per 10^{10} cm^3. More importantly, these nuclei are very short lived. Hence, it is extremely difficult to study the critical nuclei experimentally. However, it is the structure and the dynamics of these critical nuclei which play a crucial role in the nucleation process.[1–12]

The rate of crystal nucleation depends exponentially on the degree of supercooling. For this reason, a direct molecular dynamics simulation of crystal nucleation will fail at small supercooling. Under such circumstances, it is better to use a hybrid approach in which the computation of the energy barrier and the crossing rate are separated. To this end, one needs to define a 'reaction coordinate' which connects the fluid with the solid phase. Here, we follow the ideas of Van Duijneveldt and Frenkel[3] and use the orientational order parameter Q_6, as introduced by Steinhardt *et al.*[13] to act as the reaction coordinate. This order parameter is sensitive to the degree of global orientational order in the system. In the liquid there is only local orientational order, whereas the solid presents global orientational order. Hence, this order parameter is sensitive to the overall degree of crystallinity in the system. However, it is less sensitive to the difference between the possible crystalline structures. This is useful, because it implies that no particular reaction path to one of the crystalline structures that could be formed is favoured.

We can define a (Landau) Gibbs free energy as a function of this order parameter.[14]

$$G(\Phi) = \text{constant} - k_B T \ln[P(\Phi)] \tag{1}$$

where $P(\Phi)$ is the probability per unit interval of finding the order parameter around a given value of Φ. As $P(\Phi)$ is an equilibrium property of the system, it can be obtained both by Monte Carlo (MC) and molecular dynamics (MD) simulations. In order to obtain good statistics on $P(\Phi)$ even near the top of the barrier, we have applied the umbrella sampling scheme of Torrie and Valleau.[15] The main idea of this scheme is to bias the sampling of configuration space and correct for the bias afterwards. We can bias the sampling of configuration space by adding a fictitious potential to the potential of our model system. Configuration space is then sampled according to $\exp(\beta'\{U_0(q^N) + W[\Phi(q^N)]\})$, where $U_0(q^N)$ is the potential energy of the unbiased system and $W[\Phi(q^N)]$ is the biasing potential. In principle, one could use a single biasing potential to sample the entire barrier at once. However, it is usual to break up the sampling into several 'windows', each with its own biasing potential. We have taken our biasing potentials to be a harmonic function of the order parameter:

$$W[\Phi(q^N)] = \tfrac{1}{2} k_\Phi [\Phi(q^N) - \Phi_0]^2 \tag{2}$$

Note that the width and 'location' of the sampling depend on k_Φ and Φ_0. By changing the centre value of the harmonic potential, Φ_0, we can move the system from a liquid-like to a solid-like state.

In order to calculate the nucleation rate, we make use of the fact that the rate of crystallization can be considered as the product of two factors: (1) the probability of finding the system at the top of the barrier and (2) the rate with which this transition state is crossed. Denoting the transition state separating the liquid from the solid phase by Φ^*, we consider states for which $\Phi < \Phi^*$ as liquid and configurations for which $\Phi > \Phi^*$ as solid. We can now apply linear response theory,[16] to find the transition rate from the liquid to the solid state to be given by [16–19]

$$k(t) = \frac{\langle \delta(\Phi - \Phi^*) \rangle}{\langle \theta(\Phi^* - \Phi) \rangle} \frac{\langle \dot{\Phi} \delta(\Phi - \Phi^*) \theta[\Phi(t) - \Phi^*] \rangle}{\langle \delta(\Phi - \Phi^*) \rangle} = P_0(\Phi^*) R(t), \tag{3}$$

where θ is the Heaviside function.

Noting that if $\Phi < \Phi^*$ the system is in the liquid state, it is clear that $P_0(\Phi^*)$ is the probability of finding the system at the top of the barrier divided by the probability of finding it in the liquid state. It is an equilibrium property which can be measured both by MC and MD. The second contribution to the rate is $R(t)$, which is the average flux over the barrier. It is a dynamical quantity and can only be measured by MD.

From the expression in eqn. (3), we can obtain the transition-state theory approximation for the rate constant by taking the limit of $t \to 0^+$:

$$k_{TST} = \lim_{t \to 0^+} k(t) = \frac{\langle \dot{\Phi} \delta(\Phi - \Phi^*) \theta[\dot{\Phi}] \rangle}{\langle \theta(\Phi^* - \Phi) \rangle} \tag{4}$$

In transition-state theory it is assumed that all trajectories that initially are heading towards the solid, that is $\dot{\Phi}(0) > 0$, will indeed end up in the solid, and similarly, all trajectories that initially are heading towards the liquid will end up in the liquid state. This assumption is only correct if no trajectories recross the top of the barrier. The reduction of $k(t)$ by recrossing is usually indicated by the transmission κ, which is defined as:

$$\kappa = \frac{k(t)}{k_{TST}} = \frac{R(t)}{R(0^+)} \tag{5}$$

To compute the crossing rate $R(t)$, we make use of the so-called 'blue-moon ensemble'.[19,20] Constrained MD simulations are performed to generate a set of uncorrelated configurations of the system at the top of the barrier. These configurations are then used as initial states to calculate the time correlation function in $R(t)$.

2 Structure analysis

The overall crystallinity of the system can be quantified using global bond-order parameters.[13] However, it is often useful to be able to identify individual particles as solid-like or liquid-like. To this end we have developed a technique which is rather insensitive to the nature of the crystalline structure.

The analysis starts with the local orientational order parameters $\bar{q}_{lm}(i)$ defined as

$$\bar{q}_{lm}(i) \equiv \frac{1}{N_b(i)} \sum_{j=1}^{N_b(i)} Y_{lm}(\hat{r}_{ij}) \tag{6}$$

where $Y_{lm}(\hat{r}_{ij})$ are spherical harmonics, $\hat{r}_{ij}$ is a unit vector in the direction of the bond between particle i and its neighbour j and the sum runs over all $N_b(i)$ neighbours. A global order parameter, such as Q_6 is obtained by computing $\bar{Q}_{lm}$, the average of $\bar{q}_{lm}(i)$ over all particles, and then constructing rotational invariants Q_l from the $\bar{Q}_{lm}$. In the same way we can also construct local invariants:

$$q_l(i) \equiv \left(\frac{4\pi}{2l+1} \sum_{m=+l}^{1} |\bar{q}_{lm}(i)|^2 \right)^{1/2} \tag{7}$$

and

$$\hat{w}_l(i) \equiv w_l(i) \Big/ \left(\sum_{m=-l} |\bar{q}_{lm}(i)|^2 \right)^{3/2} \tag{8}$$

with $w_l(i)$ given by

$$w_l(i) \equiv \sum_{\substack{m_1, m_2, m_3 \\ m_1+m_2+m_3=0}} \begin{pmatrix} l & l & l \\ m_1 & m_2 & m_3 \end{pmatrix} \bar{q}_{lm_1}(i)\bar{q}_{lm_2}(i)\bar{q}_{lm_3}(i) \tag{9}$$

These local-order parameters are sensitive to the local order around particle i. However, the local order is large, not only in the solid, but also in the liquid. Hence, both in the liquid and in the solid the local-order parameters $q_l(i)$ are non-zero, see Fig. 1. The reason that, nevertheless, a global-order parameter, such as Q_6, vanishes in the liquid, is that all $\bar{q}_{6m}(i)$ add up incoherently. In the solid, the $\bar{q}_{6m}(i)$ add up coherently and, as a consequence, the global-order parameters are non-zero. It is precisely this phenomenon that we exploit to identify solid-like particles.

To every particle i we attribute a normalized $(2 \times 6 + 1)$-dimensional complex vector $\tilde{\boldsymbol{q}}_6(i)$, with components

$$\tilde{q}_{6m}(i) \equiv \frac{\bar{q}_{6m}(i)}{\left(\sum_{m=-6}^{6} |\bar{q}_{6m}(i)|^2 \right)^{1/2}} \tag{10}$$

We can now define a dot product of the vectors $\boldsymbol{q}_6$ of neighbouring particles i and j:

$$\boldsymbol{q}_6(i) \cdot \boldsymbol{q}_6(j) \equiv \sum_{m=-6}^{6} \tilde{q}_{6m}(i)\tilde{q}_{6m}(j)^* \tag{11}$$

By construction, $\boldsymbol{q}_6(i) \cdot \boldsymbol{q}_6(i) = 1$.

We now consider particles i and j to be 'connected' if $\boldsymbol{q}_6(i) \cdot \boldsymbol{q}_6(j)$ exceeds a certain threshold, in our case 0.5. It is clear that, in the solid, almost all $\boldsymbol{q}_6(i)$ are in-phase with

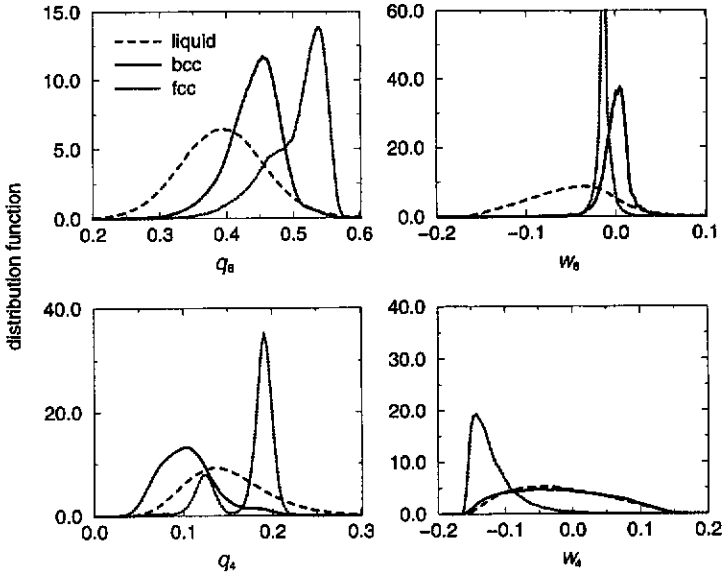

Fig. 1 Probability distribution functions of the local-order parameters, as defined in eqn. (7) and (8), in a Lennard-Jones system for a thermally equilibrated liquid, bcc and fcc structure at 20% supercooling ($P = 5.68$, $T = 0.92$). The distribution functions are based on averages over 50 independent atomic configurations.

one another and add up coherently to produce a non-zero $\bar{Q}_{6m}$. Using this criterion all particles in the solid will turn out to be connected with one another. However, we have to add another criterion. The reason is that, even in the liquid, it will frequently happen that the bond-order of a neighbouring particle is fairly coherent and thus the particles are considered to be 'connected', see Fig. 2. We, therefore, only identify a particle as solid-like if the number of connections with its neighbouring particles exceeds a thresh-

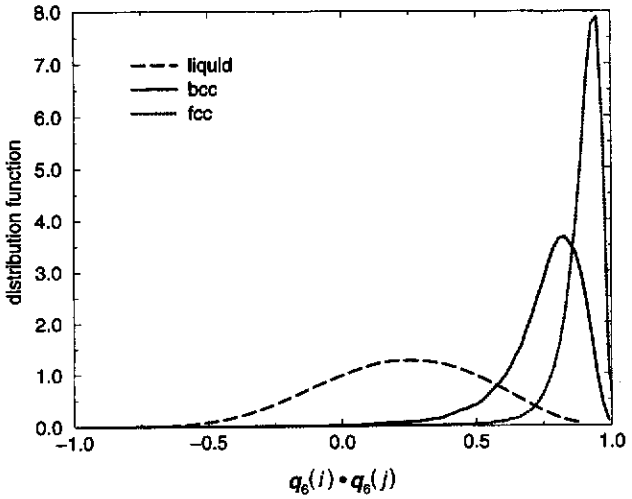

Fig. 2 Distributions of $q_6(i) \cdot q_6(j)$ of all neighbouring particles i and j for a thermally equilibrated Lennard-Jones liquid, bcc and fcc phase, at coexistence ($P = 5.68$, $T = 1.15$). Based on averages over 50 independent atomic configurations.

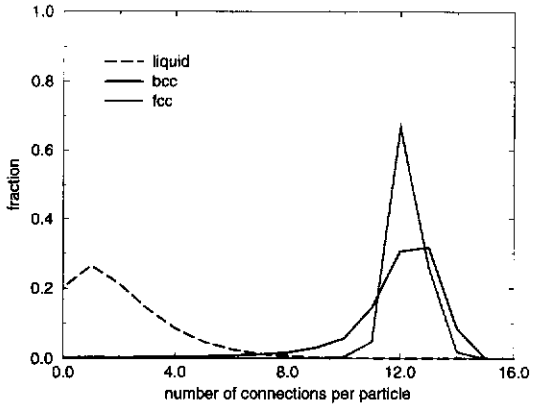

Fig. 3 Distributions of the number of connections per particle in a Lennard-Jones system for a thermally equilibrated liquid, bcc and fcc structure at coexistence ($P = 5.68$, $T = 1.15$). The distributions are based on averages over 50 independent atomic configurations.

old value. To illustrate this technique, Fig. 3 shows the histograms of the number of connections per particle for the liquid, the bcc structure and the fcc structure of the Lennard-Jones system, all equilibrated at the fcc–liquid coexistence point. As is to be expected, the average number of connections per particle is less in the liquid than in either solid. More importantly, the histogram for the liquid phase exhibits very little overlap with the histograms of the two solid phases. We find that, with a threshold value of seven connections per particle, more than 99% of the particles in an fcc structure are identified as being solid-like. Even for the bcc structure, which is rather open and disordered, this method identifies more than 97% of the particles as solid-like. In contrast, for the liquid, less than 1% of the particles were identified as being solid-like. Thus, this analysis method gives an unambiguous, local criterion to identify solid-like particles. Once we have identified the individual solid-like particles, we can perform standard cluster analysis to recognize crystallites. We apply the criterion that any two solid-like particles that are neighbours belong to the same solid cluster.

2.1 Identification of the crystalline structure

Having identified the clusters, we now wish to characterize their crystalline structure. To this end, we again make use of the local orientational order parameters. In a perfect crystal, the local bond order is the same for every particle. However, in a crystal that is equilibrated at a finite temperature, the local structure varies from one particle to another. Hence, a crystal structure equilibrated at a finite temperature will be characterized by a distribution of values of the local-order parameters, rather than by a single one. In fact, each phase has its own unique distribution. To illustrate this, we have shown in Fig. 1 the distribution functions of the local order parameters for the liquid, bcc and fcc structure. It is clear that, although the distributions are broad, there is still considerable difference between the distributions that correspond to the different phases. We therefore used these distributions as a 'fingerprint' to identify the crystal structure of the clusters.

To make the identification of a solid cluster quantitative, we have adopted the following procedure. We first determine the distribution functions of the local-order parameters in the cluster and, as reference, for the thermally equilibrated liquid, bcc and fcc structure (the local bond-order parameters, as well as the Voronoi analysis, indicated that these were the most common structures). We concatenate the distribution functions

of $q_6(i)$, $q_4(i)$ and $\hat{w}_6(i)$ [$\hat{w}_4(i)$ shows the same distribution for the liquid and bcc phase] to form a single, unique distribution function. For each structure we then associate a vector $\hat{\nu}$ with the histogram of this distribution function, where the components of this vector correspond to the bins of the histogram. We can now decompose the vector of the cluster into the characteristic vectors of the thermally equilibrated liquid, bcc and fcc structure by minimizing

$$\Delta^2 = [\hat{\nu}_{cl} - (f_{liq}\,\hat{\nu}_{liq} + f_{bcc}\,\hat{\nu}_{bcc} + f_{fcc}\,\hat{\nu}_{fcc})]^2 \tag{12}$$

where $\hat{\nu}_{cl}$, $\hat{\nu}_{liq}$, $\hat{\nu}_{bcc}$ and $\hat{\nu}_{fcc}$ are the vectors associated with the histograms of the cluster, the liquid, the bcc structure and the fcc structure, respectively. Clearly, the coefficients f_{liq}, f_{bcc} and f_{fcc} are indicative of the type of crystal structure of the cluster. The value of Δ^2 is an indication of the quality of the fit. For instance, if we were to apply our analysis to an equilibrated fcc crystal, we would find $f_{fcc} = 1, f_{bcc} = 0, f_{liq} = 0$ and $\Delta = 0$.

3 Computational details

All simulations were performed in the NPT ensemble. We carried out both MC and MD simulations. In order to keep the temperature and pressure constant in the MD simulations we employed the extended system method of Nosé and Andersen.[21] The Monte Carlo program was based on the scheme of Van Duijneveldt and Frenkel.[3] The cut-off radius for the intermolecular interactions was chosen to be 2.5. For the calculations of the bond-order parameters, the cut-off distance for nearest-neighbour bonds was 1.5, corresponding to the first minimum of $g(r)$ in an fcc crystal at coexistence. In order to have nearly spherical simulation box shape, we used truncated octahedral boundary conditions.[22]

The simulations were performed in the direction of both increasing crystallinity and decreasing crystallinity. No hysteresis was observed, although at the top of the barrier very long simulations were required to equilibrate the system. A typical simulation in a given Q_6-window consisted of an equilibration period of 10 000–50 000 cycles/timesteps, followed by a production run of 25 000–75 000 cycles/timesteps. The individual probability distribution functions of Q_6 in the different windows were fitted to a polynomial.[3] In order to determine the flux over the barrier, constrained MD was used to generate a set of 50 uncorrelated configurations at the top of the barrier. At the beginning of the unconstrained MD runs to compute $R(t)$, all particles were given a velocity drawn from a Maxwell–Boltzmann distribution and the duration of these runs was 5τ, long enough for the system to reach a stationary state.

4 Results

We studied the formation of a critical nucleus and the rate of nucleation for a Lennard-Jones system at 20% supercooling with respect to the melting temperature. A rough estimate, based on classical nucleation theory, suggests that the size of the critical nucleus is *ca.* 100 particles for this degree of supercooling. However, several studies indicate that, although the core might be quite small, the interface between the liquid and the solid is rather diffuse,[23–26] implying that the number of solid-like particles may be much larger. In order to avoid system-size artifacts, we therefore studied a rather large system of 10 648 particles.

The simulations were performed at two different reduced pressures, $P = 0.67$ and $P = 5.68$, and the data of Hansen and Verlet[27] were used to estimate the location of the melting curve. Below we discuss both the height of the energy barrier and the rate of nucleation. For both quantities we make a comparison with classical nucleation theory. Finally, we discuss the structure of the crystal nuclei.

4.1 Free energy barriers

Fig. 4 shows the free energy barriers computed for the two different pressures. Let us first describe qualitatively what happens as the top of the barrier is approached. Initially, in the liquid some small solid-like clusters are already present. When Q_6 is increased from the liquid both the number and size of the clusters increase. The reason why there are initially several small clusters instead of one, is that it is entropically favourable for the system to distribute a given amount of crystallinity over several small clusters instead of over one relatively large cluster. We discuss this in more detail below. However, as the top of the barrier is approached, the energetic factors dominate and several of the small clusters combine and form a relatively large cluster. Thus, at the top of the barrier, one large cluster, the critical nucleus, is present besides some very small ones that were already present in the supercooled liquid. This implies that the Gibbs free energy at the top of the barrier corresponds to the nucleation barrier. We can now make a comparison with classical nucleation theory.

In classical nucleation theory the height of the barrier is given by [1]

$$\Delta G^* = \frac{16\pi\gamma^3 v^2}{3(\Delta\mu)^3} \tag{13}$$

where γ is the surface energy per unit area of the liquid/crystal interface, v is the volume per particle in the solid and $\Delta\mu$ is the difference in chemical potential between the bulk solid and bulk liquid.

To obtain the difference in chemical potential we can make the approximation that, close to coexistence, it is given by[1]

$$\Delta\mu \approx \Delta h(T_m - T)/T_m \tag{14}$$

where Δh is the enthalpy change per particle on freezing at coexistence and T_m is the melting temperature. We have taken the enthalpy change from the data of Hansen and Verlet.[27] Furthermore we also need to know the interfacial free energy, γ. In fact, the surface free energy of Lennard-Jones crystals in contact with a supercooled liquid is not

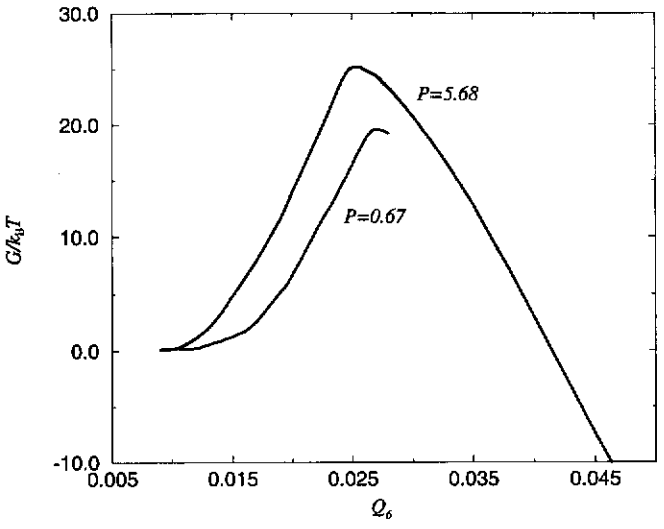

Fig. 4 Gibbs free energy of a Lennard-Jones system as a function of crystallinity (Q_6) at 20% supercooling for two different pressures, *i.e.* $P = 5.68$ ($T = 0.92$) and $P = 0.67$ ($T = 0.6$). The Gibbs free energy barriers are *ca.* $25.1k_BT$ at $P = 5.68$ and $19.4k_BT$ at $P = 0.67$.

known. However, Broughton and Gilmer[28] have calculated the interfacial free energy for the Lennard-Jones fcc/liquid interface at coexistence, near the triple point, *i.e.* $P \approx 0$.[28] If we assume that we can take the Broughton and Gilmer values for γ for our low-pressure simulations, classical nucleation theory yields the prediction $G/k_BT = 17.4$ at $P = 0.67$. Our simulations for $P = 0.67$ give $G/k_BT \approx 19.4$, which is in good agreement with the theoretical prediction. At $P = 5.68$ we cannot use the Broughton and Gilmer estimate for γ. However, if we make the assumption that the surface energy is proportional to the latent heat,[1] which increases with pressure, we arrive at an estimate of the nucleation barrier at $P = 5.68$ that is within 20% of the simulation results. So, on the whole, the agreement with classical nucleation theory is surprisingly good.

4.2 Nucleation rate

The knowledge of the energy barrier to nucleation allows us to identify the 'transition state' Q_6^*, which is the location of the maximum of the free energy. We performed MD simulations under the constraint $Q_6 = Q_6^*$, in order to generate a set of independent configurations at the top of the barrier. The structural analysis showed that all the configurations consisted of a relatively large single cluster and several small clusters of the type already present in a liquid at equilibrium. Therefore, the transition state generated in this way is very similar to the critical nucleus described in the classical theory of nucleation. These configurations were used as initial state for the computation of the time correlation function, $R(t)$ given in eqn. (3).

In Fig. 5 we have plotted the transmission coefficient κ, as defined by eqn. (5), for $P = 0.67$. If there is a single time characterizing the nucleation process, κ is expected to reach a plateau value after an initial transistory period.[16,18] In the present case, the transient period is *ca.* 0.5τ. After this time, κ remains approximately constant. It should

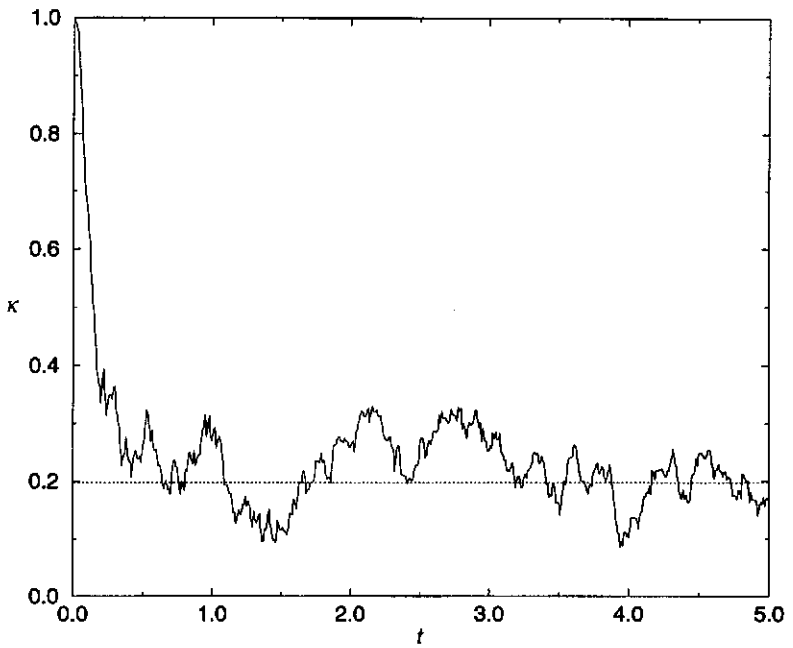

Fig. 5 Transmission coefficient as a function of time at 20% supercooling ($P = 0.67$, $T = 0.6$). The dotted line shows the plateau value that is established after 0.5τ. This figure is based on averaging over 200 trajectories.

be noticed that the statistical accuracy is rather poor, although averages were taken over 200 trajectories. This is due to the diffusive behaviour of the system at the top of the energy barrier. Analysis of the trajectories showed that in most cases the system remained rather close to the top of the barrier. This is an indication of the fact that the barrier crossing is diffusive rather than ballistic. Such a behaviour also leads to a rather small value of the transmission coefficient: $\kappa \approx 0.05$ for $P = 5.68$ and $\kappa \approx 0.2$ for $P = 0.67$.

The prediction of transition state theory for the rate can be obtained from the initial value of the flux and the results for the barrier height. It was found in the simulations that, for $P = 5.68$ $k_{TST} = 7.35 \times 10^{-14}\tau^{-1}$, and for $P = 0.67$ $k_{TST} = 2.40 \times 10^{-11}\tau^{-1}$. Combining these values with those of the transmission coefficient, we find for the nucleation rate $k = 4.04 \times 10^{-15}\tau^{-1}$ in the high-pressure case and $k = 4.79 \times 10^{-12}\tau^{-1}$ in the low-pressure case. These rates are measured in units of Q_6 per unit time. Usually the nucleation rate is measured in number of solid particles produced per unit volume per unit time. If we assume that there is a linear relation between Q_6 and the number of solid particles (which should be the case for large enough clusters) we get $k = 1.23 \times 10^{-10}\sigma^{-3}\tau^{-1}$ for $P = 5.68$ and $k = 8.19 \times 10^{-8}\sigma^{-3}\tau^{-1}$ for $P = 0.67$.

A rough estimate of the rate can also be made by making use of the diffusive character of the behaviour of the system at the top of the barrier. If we assume that a diffusive equation of the Kramers type[29] is valid, the transition rate is given by

$$k \approx \frac{D_q}{\omega} P_0(Q_6^*)$$

where D_q is the diffusion coefficient in Q_6 space close to the top of the barrier and ω is a length of the order of the barrier width. Therefore, the plateau value of $R(t)$ should be of the order of D_q/ω. We computed the diffusion coefficient D_q in the low-pressure case and found that $D_q \approx 4 \times 10^{-6}$. The width of the barrier can be estimated as $\omega \approx 5 \times 10^{-3}$, which leads to a value for the plateau $R \approx 10^{-3}\tau^{-1}$. The plateau value of $R(t)$ was found in the simulation to be $R \approx 1.4 \times 10^{-3}\tau^{-1}$. So, the description in terms of the diffusion constant is in agreement with the results of the simulations.

A final question concerning the nucleation rate is how the results of the simulation compare with the prediction of classical nucleation theory for the nucleation rate:[1,30]

$$k = A(T)\exp(-\Delta G^*/k_B T). \tag{15}$$

$A(T)$ is a kinetic prefactor and is given by

$$A(T) = Z\rho_{liq}\frac{24Dn^{*2/3}}{\lambda^2} \tag{16}$$

D is the diffusion coefficient in the liquid, ρ_{liq} is the density of the liquid, n^* is the size of the critical nucleus and λ is the atomic jump distance in the liquid. Z is the Zeldovich factor, which relates the number of solid clusters in the steady state with the equilibrium value, and is found to be

$$Z = \left(\frac{|\Delta\mu|}{6\pi k_B T n^*}\right)^{1/2} \tag{17}$$

The results of the simulations lead to a value of the Zeldovich factor of $Z = 5.12 \times 10^{-3}$ for $P = 5.68$ and $Z = 6.81 \times 10^{-3}$ for $P = 0.67$. The diffusion coefficient in the supercooled liquid was computed in a separate simulation and was found to be $D \approx 1 \times 10^{-2}\sigma^2\tau^{-1}$, for both pressures. The atomic jump distance was approximated by $\rho_{liq}^{-1/3}$, which gives $\lambda \approx 1.0\sigma$ for $P = 5.68$ and $\lambda \approx 0.97\sigma$ for $P = 0.67$. This leads to a

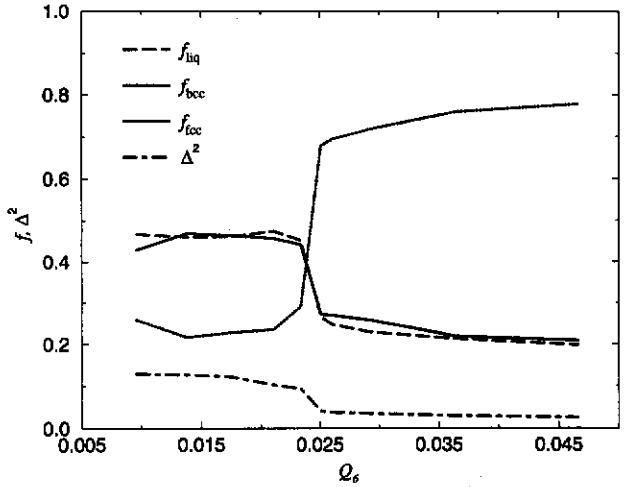

Fig. 6 Structural composition of the largest cluster present in the Lennard-Jones system, indicated by f_{liq}, f_{bcc}, f_{fcc} and Δ^2, as a function of Q_6 (the reaction coordinate) at 20% supercooling ($P = 5.68$, $T = 0.92$). This figure is based on averages over 50 independent atomic configurations.

prediction of the kinetic prefactor of $A = 8.76 \times 10^{-2}\sigma^{-3}\tau^{-1}$ for $P = 5.68$ and $A = 0.113\sigma^{-3}\tau^{-1}$ in the low-pressure case. The value of the kinetic prefactor in the simulation can easily be obtained by dividing the value of the rate k by $\exp(-\Delta G^*/k_B T)$. The resulting value is $A = 9.78\sigma^{-3}\tau^{-1}$ for $P = 5.68$ and $A = 21.83\sigma^{-3}\tau^{-1}$ for $P = 0.67$. Our simulations predict, therefore, kinetic prefactors that are about two orders of magnitude larger than predicted by classical nucleation theory. It should be mentioned that better agreement is obtained if no barrier for the addition of atoms to the critical cluster is assumed, as suggested by Broughton *et al.*[31,32]

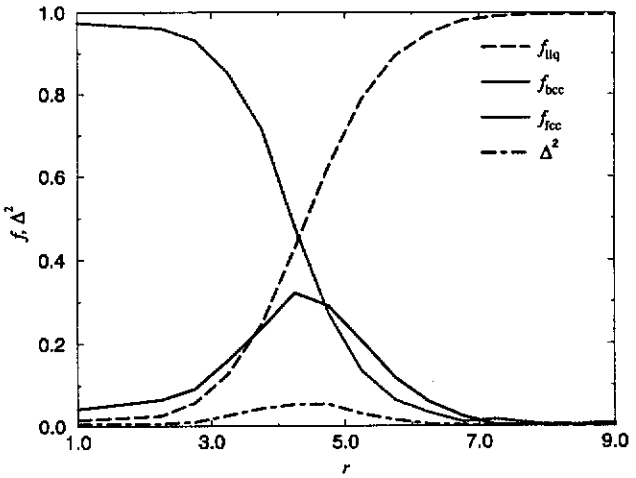

Fig. 7 Structure of a Lennard-Jones critical nucleus, indicated by f_{liq}, f_{bcc}, f_{fcc} and Δ^2, as a function of r, the distance to its centre-of-mass, at 20% supercooling ($P = 5.68$, $T = 0.92$). This figure is based on averages over 50 independent atomic configurations.

4.3 Structure of the nuclei

Fig. 6 shows the structural composition of the largest cluster in our system , as a function of our reaction coordinate Q_6 (the results shown are for $P = 5.68$. The $P = 0.67$ results are similar). The figure shows that the precritical nuclei are predominantly bcc and liquid-like. The fact that they have a high liquid character is not surprising as the clusters are very small, ranging from 16 particles in the metastable liquid to 30 particles as the top of the barrier is approached. What is more interesting is that they are clearly more bcc ordered than that they are fcc ordered. This suggests that, at least for the small crystallites, we find the behaviour as predicted by the Alexander–McTague scenario,[4] who argued that, in 3D nucleation, the bcc phase is uniquely favoured over all other possible crystalline phases. However, as the critical and postcritical nuclei are increasingly fcc-like, our results are also in agreement with the findings of Swope and Andersen,[11] who found that nucleation in a Lennard-Jones system mainly proceeded *via* fcc crystallites.

However, the critical and postcritical nuclei are not completely fcc ordered but have a high degree of bcc and liquid-like character. Again, the fact that they have a high degree of liquid character is not surprising as these nuclei are still relatively small, ranging from 600 particles for the critical nucleus to 1400 particles for the postcritical nucleus at $Q_6 = 0.045$. However, the bcc character is less expected. We therefore studied the local order of the critical and postcritical nuclei in more detail, which is facilitated by the fact that we find these nuclei to be quite spherical.

Given the spherical shape of the critical and postcritical nuclei we have calculated the structural composition as a function of r, the distance to the centre-of-mass. Fig. 7 shows f_{liq}, f_{bcc} and f_{fcc} as a function of r for the critical nucleus. As expected, we see that the core of the critical nuclei is mainly fcc ordered and that f_{fcc} and f_{liq} go smoothly to zero and one in the liquid, respectively. However, the fraction of bcc atoms increases in the interface before it decays to zero in the liquid. Hence, the present results show that the fcc core is covered by a shell which has more bcc character. This finding also explains why the precritical nuclei have a high degree of bcc ordering: they are so small that they are only interface. Furthermore, note that it is also compatible with the observation that the critical nuclei and postcritical nuclei still have considerable bcc character: our method of identifying solid-like particles also identifies in the interface as being part of the cluster.

To summarize the evolution of the size and the structure of the nuclei as the order parameter is increased from the liquid: initially we have small nuclei that are predominantly bcc and liquid ordered. As the top of the barrier is approached, these small nuclei merge and form one large cluster, the critical nucleus. The core of this nucleus is mainly fcc ordered. However, a high degree of bcc ordering in the interface is retained.

Nevertheless, one question cannot be answered yet and that is: what is the structure of a large but precritical nucleus? At the precritical side we always have several small clusters, and never one relatively large cluster. In the next section we will discuss this problem in more detail.

5 One or many crystallites?

When a liquid phase solidifies, it will tend to form the solid structure with the lowest free energy. It is usually assumed that the lowest free energy state in the two-phase region is one in which a single large crystallite has formed. The reason why this is the lowest free energy state is, of course, that a single crystal has a lower surface area than a larger number of crystallites with the same total volume. And, indeed, it seems obvious that once crystallization is complete, the single crystal must correspond to the (overwhelmingly) most likely situation.

However, in a simulation, we can constrain a system to be at a given point in the two-phase region. That is, the crystalline phase takes up a fixed volume fraction ϕ_{cr} of the total available volume. The question is: is the single crystal still, necessarily, the most stable configuration?

In the early work of Salsburg and Wood,[33] the barrier that is responsible for hysteresis in constant NVT simulations is estimated assuming that a system in the two-phase region will always try to minimize its surface free energy. However, one should also consider the fact that by breaking up a single crystal into a large number of smaller crystallites, the system may gain entropy. The question is if and when this entropic gain outweighs the surface free energy cost.

To arrive at an estimate, we consider the following simple model. The total Helmholtz free energy of a system consisting of M particles (of which N particles are in the solid phase) in volume V at temperature T, is denoted by F. The fraction of all particles that are in the crystalline state is

$$X_{cr} = N/M \tag{18}$$

Let us now compute the excess free energy per solid-like particle in a two-phase system, using the Helmholtz free energy of the neat liquid as our reference state. The Helmholtz free energy of the two-phase system contains three contributions:

1. A negative 'bulk' contribution

$$\frac{\beta F_b}{N} = -\Delta\beta\mu \tag{19}$$

where $\Delta\mu$ is the chemical potential difference between solid and liquid and $\beta = 1/k_B T$. This term does not change as we redistribute particles over different numbers of crystallites. We need not consider this term in the rest of our analysis.

2. A surface free energy term,

$$\frac{\beta F_s}{N} = \frac{n_{cr}}{N} 4\pi r_c^2 \beta\gamma_{sl} \tag{20}$$

where n_{cr} is the number of crystallites, r_c is the crystallite radius and γ_{sl} is the free energy per unit area of the solid/liquid interface. We can easily relate r_c to the volume fraction occupied by the solid:

$$n_{cr}\rho_{cr}(4\pi/3)r_c^3 = N \tag{21}$$

where ρ_{cr} is the number density of the crystal. Hence,

$$r_c = [N(3/4\pi\rho_{cr} n_{cr})]^{1/3} \tag{22}$$

If we insert this in the expression for F_s, we obtain

$$\frac{\beta F_s}{N} = \frac{n_{cr}}{N} 4\pi\beta\gamma_{sl}[N(3/4\pi\rho_{cr} n_{cr})]^{2/3} = \left(\frac{n_{cr}}{N}\right)^{1/3} 4\pi\beta\gamma_{sl}[(3/4\pi\rho_{cr})]^{2/3} \tag{23}$$

$$\equiv \left(\frac{n_{cr}}{N}\right)^{1/3} \beta f_0 \tag{24}$$

The last line defines the parameter

$$f_0 \equiv 4\pi\gamma_{sl}[(3/4\pi\rho_{cr})]^{2/3} \tag{25}$$

For the Lennard-Jones system near the triple point, βf_0 is a number of order 1.

3. The final term is a translational entropy term.† To estimate this term, we simply assume that the crystallites behave like a gas of identical spherical particles. The free energy of such a gas could, for instance, be estimated using the Carnahan–Starling equation of state. However, we shall assume that the volume fraction of solid is low, and we therefore ignore all non-ideal terms in this free energy.

$$\frac{\beta F_{\mathrm{tr}}}{N} \approx \frac{n_{\mathrm{cr}}}{N} [\ln(n_{\mathrm{cr}}/V) - 1] \tag{26}$$

It is convenient to rewrite the above expressions in terms of n_0, the number of particles per crystallite ($n_0 = N/n_{\mathrm{cr}}$). If we combine the surface and translational free energies, we get:

$$\frac{\beta F(n_{\mathrm{cr}})}{N} = \frac{1}{n_0^{1/3}} \beta f_0 + \frac{1}{n_0} \left[\ln\left(\frac{N/V}{n_0}\right) - 1 \right] \tag{27}$$

Rather than carry out the minimization of the energy with respect to n_0, we consider two limiting cases, namely $n_0 = N$ ($n_{\mathrm{cr}} = 1$), *i.e.* a single crystallite and $n_{\mathrm{cr}} = N_{\max}$, a total break-up of the solid into small 'nano' crystallites. The smallest cluster should still be large enough to be recognized as a crystal. Hence, we should expect that there will be of the order of 12 particles in the minimal solid cluster. We call this number $n_{\min}$. Hence $N_{\max} = N/n_{\min}$.

Before we proceed we should reconsider the 'neat' liquid at coexistence. Even in the liquid there will be a finite concentration of small clusters or, what amounts to the same thing, the average number of crystalline particles ($\langle N \rangle_l$) is non-zero in the liquid. As we move into the two-phase region, the number of crystalline particles increases and we should look at the initial change in energy.

To estimate $\langle n_{\mathrm{cr}} \rangle_l$, the number of nano-crystallites in the neat fluid, we consider the expression for the free energy as a function of n_{cr}:

$$\beta F_l = n_{\mathrm{cr}}[n_{\min}^{2/3} \beta f_0 + \ln(n_{\mathrm{cr}}/V) - 1] \tag{28}$$

To find the state of lowest free energy, we minimize with respect to n_{cr}, to find

$$\beta f_0 n_{\min}^{2/3} + \ln\left(\frac{n_{\mathrm{cr}}}{V}\right) = 0 \tag{29}$$

Hence, the equilibrium concentration of nano-crystallites in the neat fluid is

$$\langle n_{\mathrm{cr}}/V \rangle_l = \exp(-\beta f_0 n_{\min}^{2/3}) \tag{30}$$

The second derivative of the free energy with respect to n_{cr} is

$$\frac{\partial^2 \beta F}{\partial n_{\mathrm{cr}}^2} = \frac{1}{n_{\mathrm{cr}}} \tag{31}$$

Therefore, close to coexistence, the dependence of the free energy on the number of crystalline particles is given by

$$\Delta \beta F = \frac{\exp(\beta f_0 n_{\min}^{2/3})}{2V n_{\min}^2} (\Delta N)^2 \tag{32}$$

† In what follows, we ignore the entropic contribution due to the integral degrees of freedom of the cluster.[34]

or, in terms of the fraction of crystalline material $X_{cr} = (\Delta N)/M$

$$\beta\Delta F = \frac{V \exp(\beta f_0 n_{min}^{2/3})\rho^2}{2n_{min}^2} X_{cr}^2 \tag{33}$$

Now consider the alternative scenario where all additional crystalline material is used to form a single cluster. The radius of this large cluster is related to the radius of the nano-clusters by

$$r_{large}^3 = r_{nano}^3(\rho V X_{cr})/n_{min} \tag{34}$$

and then

$$\beta\Delta F = f_0\left(\frac{\rho V X_{cr}}{n_{min}}\right)^{2/3} \tag{35}$$

Note that the free energy of a single cluster varies as $X_{cr}^{2/3}$. Hence, initially it is always more favourable to form many small crystallites, rather than a single large one. Let us now estimate the point where the single cluster becomes more stable. This happens when

$$f_0\left(\frac{\rho V X_{cr}}{n_{min}}\right)^{2/3} = \frac{V \exp(\beta f_0 n_{min}^{2/3})\rho^2}{2n_{min}^2} X_{cr}^2 \tag{36}$$

This implies that

$$X_{cr}^{4/3} = f_0\left(\frac{\rho}{n_{min}}\right)^{2/3} \frac{2n_{min}^2}{\exp(\beta f_0 n_{min}^{2/3})\rho^{2-}} V^{-1/3} \tag{37}$$

or

$$X_{cr} \sim V^{-1/4} \tag{38}$$

This means that the break-even point depends on system size. For computer simulations of finite systems, this effect is certainly non-negligible, as illustrated by our simulation results. A more general problem with the use of such a 'global' measure for the degree of crystallinity is that the size of the smallest cluster that is stable with respect to entropic break-up grows with system size:

$$N_{large} = \rho\left(\frac{\rho}{n_{min}}\right)^{1/2}\left(\frac{2f_0 n_{min}^2}{\exp(\beta f_0 n_{min}^{2/3})\rho^2}\right)^{3/4} V^{3/4} \tag{39}$$

Therefore, even if a cluster is 'postcritical' in the sense of classical nucleation theory, it may still be 'precritical' for entropic reasons.

We emphasize that the above derivation is oversimplified. However, it shows that problems may arise when using a global (*i.e.* total degree of crystallinity) rather than local (*i.e.* size of the largest cluster) order parameter in the construction of the free energy barrier between liquid and solid.

6 New method

In our simulations we found that large precritical nuclei are not stable on the liquid side of the barrier unless the system is close to the top. We therefore devised a new method which enables us to grow a single cluster all the way from the liquid to the solid. Rather

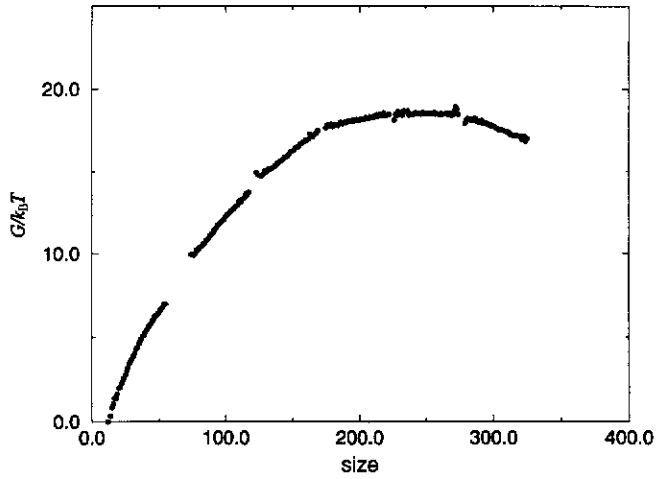

Fig. 8 Gibbs free energy of the $r^{-12.5}$ system as a function of the size of the largest cluster present in the system at 25% supercooling ($P = 22.54$, $T = 0.75$)

than using a global-order parameter, which is sensitive to the overall degree of crystallinity in the system, we took as the order parameter the size of the largest cluster in the system. The advantage of this scheme is that we can directly control the size of the nucleus we want to study. In order to determine the size of the cluster, we use the techniques to identify solid clusters as explained in Section 2. As our method of identifying solid-like particles is rather insensitive to the type of ordering, we do not favour one crystalline structure over the other.

In order to test the new method we performed NPT MC simulations on a system consisting of soft repulsive spheres, interacting *via* $v(r) = \varepsilon(\sigma/r)^n$, with $n = 12.5$. The degree of supercooling was 25% with respect to the coexistence point given by Agrawal and Kofke.[35] The number of particles was $N = 3456$, which was large enough to avoid serious finite-size effects.

In order to sample all cluster sizes with the same frequency we again used the umbrella sampling scheme. The biasing potential function was again taken to be a harmonic function of the order parameter, which is now the size of the cluster. In principle, one could recalculate the size of the cluster after every trial displacement of a particle. However, this is computationally expensive. We therefore adopted a different procedure. We first perform a sequence of unbiased MC cycles, that is, according to the potential of the original system, $U(\boldsymbol{q}^N)$. We then recalculate the size of the cluster and accept the trajectory according to $\exp\{-\beta\Delta W[\Phi(\boldsymbol{q}^N)]\}$, where $\Delta W[\Phi(\boldsymbol{q}^N)]$ is the difference in biasing potential before and after the sequence of unbiased MC cycles. This ensures that we generate configurations according to $\exp(\beta\{U(\boldsymbol{q}^N) + W[\Phi(q^N]\})$.

Fig. 8 shows the Gibbs free energy of the system as a function of the size of the largest cluster present in the system. The Gibbs free energy of the system can be identified with the Gibbs free energy of this cluster as there is always only one large solid cluster present in the system. In order to illustrate this we have shown, in Fig. 9, a snapshot of all solid-like particles in the system when it is at the liquid side of the barrier. The large solid cluster in the middle of the box, comprising 150 particles, is clearly seen. To show the difference from the old method, we have taken this configuration as the starting configuration for a run using the old, global-order parameter Q_6. In Fig. 10 the size of the largest cluster present in the system is given as a function of 'time'. Initially, the size of the cluster drops because the system has to adjust itself to the

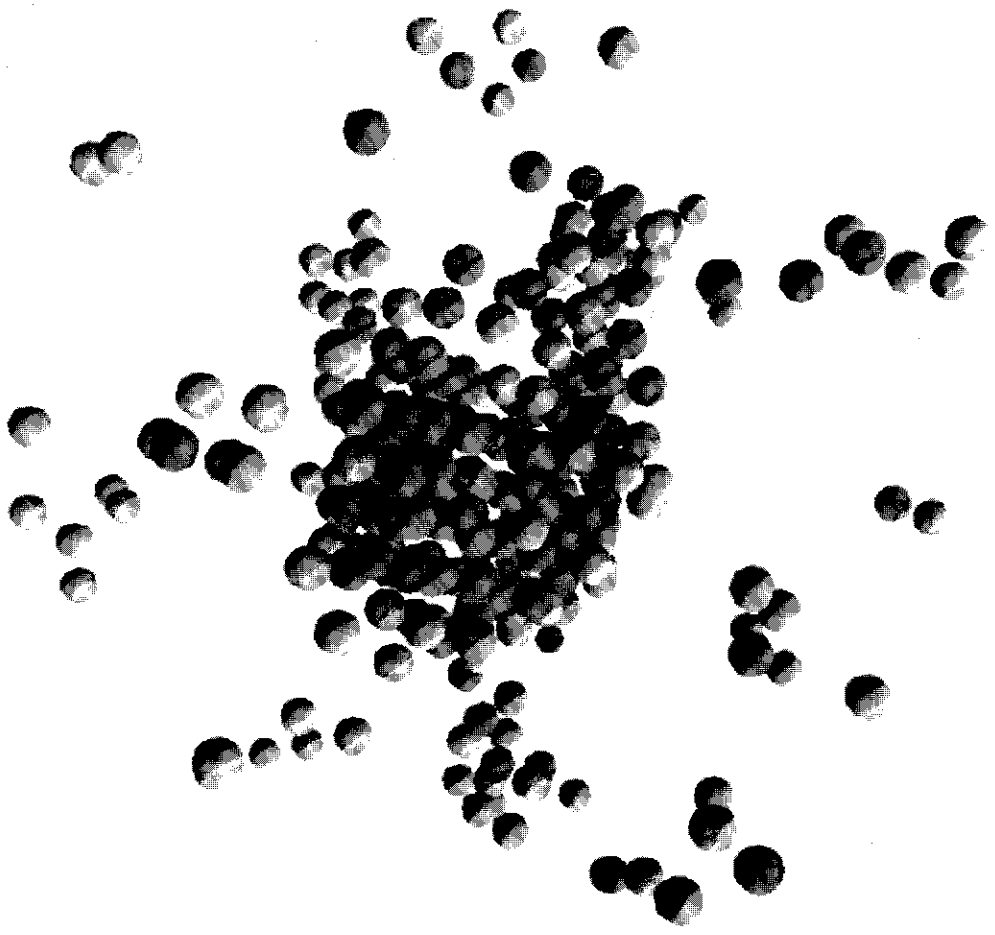

Fig. 9 Snapshot of all solid particles in the $r^{-12.5}$ system at the precritical side of the nucleation barrier, at 25% supercooling ($P = 22.54$, $T = 0.75$). The size of the large solid cluster in the middle is 150 particles.

new biasing potential. The size of the cluster then fluctuates for 5000 cycles. Then, however, the size suddenly decreases to reach a new, much smaller plateau value. It is clear that using the global-order parameter Q_6 the large precritical nucleus breaks up into many small crystallites. In fact, the process is 'reversible', that is, if we use as the starting configuration for a run with the new order parameter, a configuration with only many small clusters and not a single relatively large cluster, we finally end up with a configuration containing one relatively large cluster, and some very small clusters that are always present in the supercooled liquid.

In summary, using a combination of umbrella sampling and 'blue-moon' ensemble simulations, it is possible to compute crystal nucleation rates at moderate supercooling. However, it is useful to choose a local rather than a global order parameter as a reaction coordinate, because in the case of a global-order parameter, crystal nuclei may spontaneously break up for entropic reasons.

This work was supported in part by 'Scheikundig Onderzoek Nederland' (SON) with financial aid from NWO ('Nederlandse Organisatie voor Wetenschappelijk

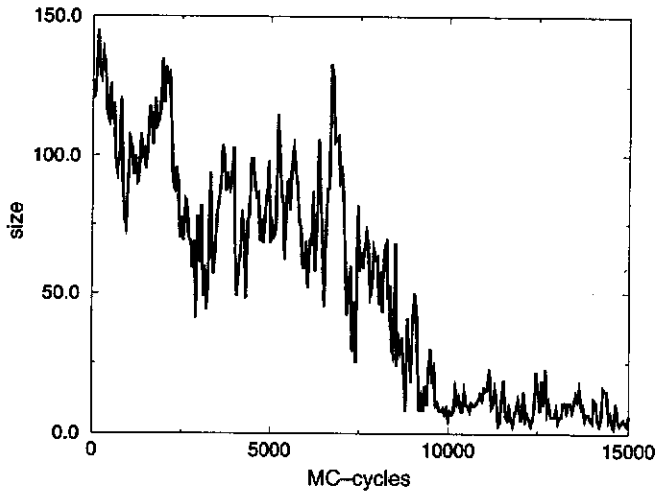

Fig. 10 Size of the largest cluster present in the system as a function of the number of MC cycles using the old global-order parameter Q_6. As the starting configuration we have taken the precritical configuration that is obtained with the new scheme, see Fig. 9.

Onderzoek"). The work of the FOM Institute is part of the research program of "Stichting Fundamenteel Onderzoek der Materie" (FOM) and is supported by NWO. Part of the computation reported in this work was supported through NWO grant MPR-94.2186. M.J.R.M. acknowledges partial support from EU-HCM Grant Nr. ERBCHWICT941060 and Grant No. PB92-0683 from Dirección General de Investigación Científica y Técnica (Spain).

References

1 K. F. Kelton, in *Solid State Physics*, ed. H. Ehrenreich and D. Turnbull, Academic, Boston, 1991, vol. 45, 75–177.
2 D. W. Oxtoby, *J. Phys. Condens. Matter*, 1992, **4**, 7627.
3 J. S. van Duijneveldt and D. Frenkel, *J. Chem. Phys.*, 1992, **96**, 4655.
4 S. Alexander and J. P. McTague, *Phys. Rev. Lett.*, 1978, **41**, 702.
5 W. Klein and F. Leyvraz, *Phys. Rev. Lett.*, 1986, **57**, 2845.
6 R. E. Cech, *J. Metall.*, 1956, **8**, 585.
7 H-M. Lin, Y-W. Kim and T. F. Kelly, *Acta Metall.*, 1988, **36**, 2537.
8 M. J. Mandell, J. P. McTague and A. Rahman, *J. Chem. Phys.*, 1976, **64**, 3699.
9 C. S. Hsu and A. Rahman, *J. Chem. Phys.*, 1979, **71**, 4974.
10 J. Yang, H. Gould and W. Klein, *Phys. Rev. Lett.*, 1988, **60**, 2665.
11 W. C. Swope and H. C. Andersen, *Phys. Rev. B.*, 1990, **41**, 7042.
12 P. R. ten Wolde, M. J. Ruiz-Montero and D. Frenkel, *Phys. Rev. Lett.*, 1995, **75**, 2714.
13 P. J. Steinhardt, D. R. Nelson and M. Ronchetti, *Phys. Rev. B*, 1983, **28**, 784.
14 L. D. Landau and E. M. Lifshitz, *Statistical Physics*, Pergamon, London, 3rd edn., 1980.
15 G. M. Torrie and J. P. Valleau, *Chem. Phys. Lett.*, 1974, **28**, 578.
16 D. Chandler, *Introduction to Modern Statistical Mechanics*, Oxford University Press, New York, 1987.
17 C. H. Bennett in *Algorithms for Chemical Computations*, ed. R. E. Christofferson, American Chemical Society, Washington, 1977.
18 D. Chandler, *J. Chem. Phys.* 1978, **68**, 2959.
19 E. A. Carter, G. Ciccotti, J. T. Hynes and R. Kapral, *Chem. Phys. Lett.*, 1989, **156**, 472.
20 G. Ciccotti, in *Computer Simulations in Materials Science*, ed. M. Meyer and V. Pontikis, Kluwer, Dordrecht, 1991, pp. 119–137.
21 S. Nosé, in *Computer Simulations in Materials Science*, ed. M. Meyer and V. Pontikis, Kluwer, Dordrecht, 1991, pp. 21–41.
22 D. J. Adams, *CCP5 Quarterly*, 1983, **10**, 30.
23 P. Harrowell and D. W. Oxoby, *J. Chem. Phys.*, 1984, **80**, 1639.
24 M. J. Mandell, J. P. McTague and A. Rahman, *J. Chem. Phys.*, 1977, **66**, 3070.

25 J. D. Honeycutt and H. C. Andersen, *J. Phys. Chem.*, 1986, **90**, 1585.
26 C. K. Bagdassarian and D. W. Oxotoby, *J. Chem. Phys.*, 1994, **100**, 2139.
27 J. P. Hansen and L. Verlet, *Phys. Rev.*, 1969, **184**, 151.
28 J. Q. Broughton and G. H. Gilmer, *J. Chem. Phys.*, 1986, **84**, 5759.
29 H. A. Kramers, *Physica*, 1940, **7**, 284.
30 D. Turnbull and J. C. Fisher, *J. Chem. Phys.*, 1949, **17**, 71.
31 J. Q. Broughton, G. H. Gilmer and K. A. Jackson, *Phys. Rev. Lett.*, 1982, **49**, 1496.
32 E. Burke, J. Q. Broughton and G. H. Gilmer, *J. Chem. Phys.*, 1988, **89**, 1030.
33 Z. W. Salsburg and W. W. Wood, *J. Chem. Phys.*, 1962, **37**, 798.
34 M. E. Fisher, *Physics*, 1967, **3**, 255.
35 R. Agrawal and D. A. Kofke, *Mol. Phys.*, 1995, **85**, 23.

Paper 6/03261C; *Received* 9*th May*, 1996